

Effect of magnetization inhomogeneity on magnetic microtraps for atoms

S. Whitlock, B. V. Hall,* T. Roach, R. Anderson, P. Hannaford, and A. I. Sidorov
*ARC Centre of Excellence for Quantum-Atom Optics and
 Centre for Atom Optics and Ultrafast Spectroscopy,
 Swinburne University of Technology, Hawthorn, Victoria 3122, Australia*
 (Dated: September 19, 2018)

We report on the origin of fragmentation of ultracold atoms observed on a magnetic film atom chip. Radio frequency spectroscopy and optical imaging of the trapped atoms is used to characterize small spatial variations of the magnetic field near the film surface. Direct observations indicate the fragmentation is due to a corrugation of the magnetic potential caused by long range inhomogeneity in the film magnetization. A model which takes into account two-dimensional variations of the film magnetization is consistent with the observations.

PACS numbers: 03.75.Be, 07.55.Ge, 34.50.Dy, 39.25.+k

An atom chip is designed to manipulate magnetically trapped ultracold atoms near a surface using an arrangement of microfabricated wires or patterned magnetic materials [1]. Since the realization of Bose-Einstein condensates (BECs) on atom chips [2, 3], pioneering experiments have studied single-mode propagation along waveguides [4], transport and adiabatic splitting of a BEC [5] and recently on-chip atom interferometry [6, 7]. Permanent magnets are particularly attractive for atom chips as they can provide complex magnetic potentials [8] while suppressing current noise that causes heating and limits the lifetime of trapped atoms near a surface [9]. To date, permanent magnet atom chips have been developed with a view to study one-dimensional quantum gases [10, 11, 12], decoherence of BEC near surfaces [9, 13], hybrid magnetic and optical trapping configurations [14], and self biased fully permanent magnetic potentials [15]. It has been found, however, that in addition to current noise, atom chips have other limitations, as undesired spatial magnetic field variations associated with the current-carrying wires or magnetic materials act to fragment the trapped atoms.

In previous work, fragmentation of atoms trapped near current-carrying wires was traced to roughness of the wire edges that causes tiny current deviations [16, 17]. This introduces a spatially varying magnetic field component parallel to the wire which corrugates the bottom of the trap potential. While more advanced microfabrication techniques have been used to produce wires with extremely straight edges, thereby minimizing fragmentation [18, 19], the first experiments with permanent magnet atom chips have now also indicated the presence of significant fragmentation [12, 20, 21]. This has motivated further work towards understanding the mechanisms that cause fragmentation near magnetic materials.

In this paper we report on the origin of fragmentation near the surface of a permanent magnetic film atom chip. To characterize the magnetic field near the film surface

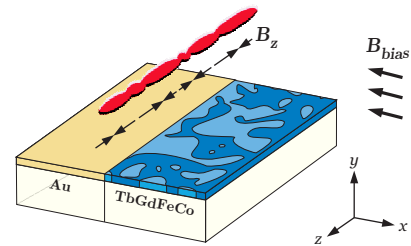


FIG. 1: (Color online) Schematic diagram of our permanent magnetic film atom chip. Inhomogeneity in the film magnetization leads to fragmentation of the trapped cloud of ultracold atoms when positioned near the surface.

we have developed a technique which combines precision radio frequency (rf) spectroscopy of trapped atoms with high spatial resolution optical imaging. This allows sensitive and intrinsically calibrated measurements of the magnetic field landscape to be made over a large area. We find the fragmentation originates from long range inhomogeneity in the film magnetization and has characteristics that differ from those observed for current-carrying wire atom chips. To account for the observations we have developed a model for the spatial decay of random magnetic fields from the surface due to inhomogeneity in the film magnetization.

A schematic diagram of a basic magnetic film atom chip is shown in Fig. 1. Our atom chip uses a $\text{Tb}_6\text{Gd}_{10}\text{Fe}_{80}\text{Co}_4$ film which exhibits strong perpendicular anisotropy [13]. The edge of the $300\ \mu\text{m}$ thick glass-slide substrate is polished to optical quality prior to film deposition. Scanning profilometer measurements on similarly prepared substrates indicate that the residual edge roughness is less than $50\ \text{nm}$ and the top surface is extremely smooth. The substrate is sputter-coated with a multilayer magnetic film ($6 \times 150\ \text{nm}$ TbGdFeCo and $6 \times 140\ \text{nm}$ Cr) and a gold overlayer ($100\ \text{nm}$), and the film topology accurately follows that of the polished substrate. The deposited film has been analyzed using a SQUID magnetometer and a magnetic force microscope (MFM) and has shown excellent magnetic properties [22].

*Electronic address: brhall@swin.edu.au

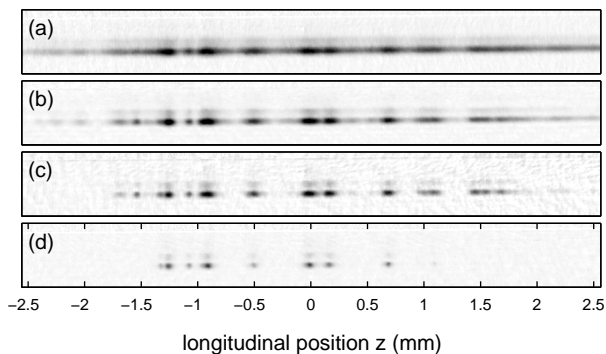


FIG. 2: Absorption images of the atomic density in the magnetic microtrap located $y_0 = 67 \mu\text{m}$ from the surface. As the rf cut-off ν_f is decreased, the structure of the potential is revealed. (a) $\nu_f = 1238 \text{ kHz}$, (b) $\nu_f = 890 \text{ kHz}$, (c) $\nu_f = 766 \text{ kHz}$, (d) $\nu_f = 695 \text{ kHz}$.

The film is magnetized perpendicular to the surface by a magnetic field of 1 T and afterwards is magnetically homogeneous within the sensitivity of the MFM. A second glass slide, coated with a non-magnetic gold film, completes the reflective atom chip surface (Fig. 1). Both substrates are then epoxied to a $500 \mu\text{m}$ thick silver foil current-carrying structure which is used for loading ultracold atoms into the permanent magnet microtrap, to provide weak longitudinal confinement, and as an in-built radio frequency antenna.

At the edge of the perpendicularly magnetized film a field is produced that is analogous to that of a thin current-carrying wire aligned with the film edge ($I_{eff} = 0.2 \text{ A}$) [8, 13]. A magnetic microtrap is formed by the field from the film, a uniform magnetic field B_{bias} , and two current-carrying end-wires. In the experiment 2×10^8 ^{87}Rb atoms are collected in a mirror magneto-optical trap located 5 mm from the surface. These atoms are optically pumped to the $|F = 2, m_F = +2\rangle$ hyperfine state and subsequently transferred to a magnetic trap formed by a Z-shaped current-carrying wire and B_{bias} . A preliminary rf evaporative cooling stage is used to reduce the cloud temperature below $5 \mu\text{K}$. The remaining atoms are then transferred to the magnetic film microtrap by adiabatically reducing the current through the Z-shaped wire to zero. The final values of B_{bias} vary from 0.2 mT to 0.8 mT , so the transverse trap frequency varies between $2\pi \times 410 \text{ Hz}$ and $2\pi \times 1500 \text{ Hz}$ while the trap position y_0 ranges from $200 \mu\text{m}$ to $50 \mu\text{m}$ from the surface. The end-wires are operated at 0.5 A such that the trap depth is $\sim 100 \mu\text{K}$ and the elongated cloud of atoms extends 5 mm along the edge of the atom chip to allow measurement of the magnetic potential.

The narrow energy distribution of ultracold atoms is an inherent advantage when used as a probe of weak potentials. In particular, the equilibrium distribution of trapped atoms has been used to image magnetic fields near test wires with high sensitivity and high spatial resolution [23, 24]. In parallel, rf spectroscopy has been

used as a precise and powerful method for investigating the properties of cold atom clouds [25, 26, 27, 28, 29]. In this paper we use rf spectroscopy of ultracold atoms to accurately profile small magnetic field variations near the magnetic film surface.

A spatially uniform rf field of frequency ν is applied perpendicular to the trap axis to resonantly outcouple atoms to untrapped magnetic states at positions where $g_F \mu_B |B(x, y, z)| = h\nu$. The rf field is swept using a single frequency ramp ($\sim 0.2 \text{ MHz/s}$) from 2 MHz to a final cut-off frequency ν_f ranging between 1.4 MHz and 0.5 MHz . The Rabi frequency of the rf transition is $2\pi \times 0.5 \text{ kHz}$, high enough to ensure that atoms with total energy greater than $h\nu$ are removed from the trap with high probability and that regions of the potential where $g_F \mu_B |B(x, y, z)| \geq h\nu$ thereafter remain unpopulated. During the early stages of the rf sweep the cloud undergoes some evaporative cooling as the in-trap collision rate is high enough to allow rethermalization. At the end of the sweep the resonant frequency approaches that corresponding to the trap bottom and the cloud becomes significantly truncated by the rf field.

Immediately after the sweep, B_{bias} is switched off to accelerate the atoms away from the film surface in the remaining permanent magnetic field gradient. The longitudinal density distribution is unperturbed during the 1 ms expansion time and is an accurate representation of the in-trap distribution. A resonant absorption image is then recorded by a CCD with a spatial resolution of $5 \mu\text{m}$. A series of absorption images for different values of ν_f is shown in Fig. 2. Noticeable fragmentation is observed when ν_f is reduced below 1.3 MHz (Fig. 2a). For $\nu_f \sim 0.9 \text{ MHz}$ the density distribution becomes truncated by the rf field and regions of the atomic density decrease to zero (Fig. 2b). Reducing ν_f further results in well separated clumps of atoms which are found only in the lowest potential wells (Fig. 2c, d).

For a quantitative analysis we assume that the full trapping potential can be expressed in terms of the transverse confinement and the corrugated longitudinal potential $m_F g_F \mu_B |B_z(z) + B_0|$ where B_0 is the value of the uniform offset field [17]. The atomic distribution in the trap immediately after the rf sweep is described by a truncated Boltzmann distribution [26, 30]. To extract $|B_z(z) + B_0|$, the integrated atomic density as a function of ν_f can be fit for each position z to the truncated thermal distribution function,

$$n(z, \beta) = n_\infty(z) [\text{erf}(\sqrt{\beta}) - 2\sqrt{\beta/\pi} e^{-\beta} (1 + 2\beta/3)], \quad (1)$$

where n_∞ is the integrated atom density before truncation and the spatially dependent truncation parameter β is

$$\beta(z, \nu_f) = (m_F h \nu_f - m_F g_F \mu_B |B_z(z) + B_0|) / k_B T, \quad (2)$$

where T is a fit parameter, which characterizes the non-equilibrium distribution during truncation. We find however that this model does not satisfactorily reproduce the

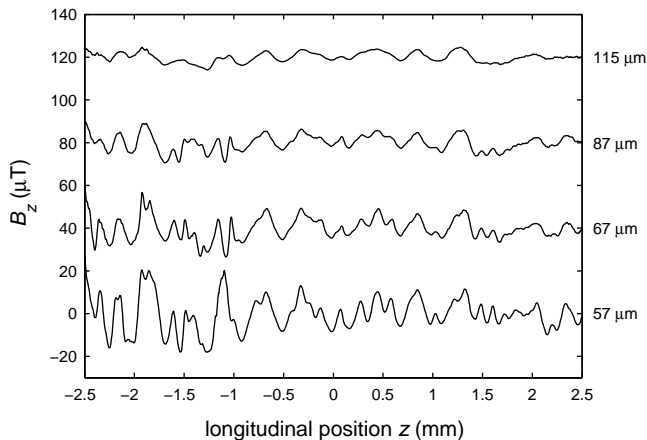


FIG. 3: Magnetic field profiles measured using spatially resolved rf spectroscopy for various distances to the surface. The field offset B_0 and the effect of weak longitudinal confinement are subtracted and each profile has been offset by $40 \mu\text{T}$ for clarity.

density distribution in regions of the potential where the atomic density becomes large; specifically at the bottom of each potential well for lower values of ν_f . To minimise this effect we section the full data set into $80 \mu\text{m}$ spatial regions and fit Eq. (1) using a two-dimensional minimisation algorithm as opposed to fitting for each value of z independently. This effectively constrains the fitted truncation temperature T to vary smoothly over a range corresponding roughly to the extent of a potential well. After reconstructing the magnetic field profile the effect of the end-wires is subtracted. The statistical uncertainty in the measurement is approximately $0.1 \mu\text{T}$, which is mainly attributed to fluctuations of external magnetic fields. With appropriate magnetic shielding the expected sensitivity of the technique is limited by the power broadened rf linewidth required to effectively outcouple atoms.

Complete magnetic field profiles are given for several distances from the film in Fig. 3. Firstly, the amplitude and structure of the corrugated potential are constant from day to day; however the amplitude increases as the trap is positioned closer to the surface, with an approximate power law dependence given by y^{-a} , where $a = 1.8 \pm 0.3$. For $y_0 > 100 \mu\text{m}$ the potential has a characteristic period of about $390 \mu\text{m}$, significantly longer than that commonly observed near electroplated wires [17, 31]. Closer to the film, additional corrugations appear with a characteristic period of about $170 \mu\text{m}$. These y -dependent characteristics of the potential have allowed time-dependent manipulation of BECs at particularly interesting regions of the disordered potential [32].

The figure of merit for corrugation observed above the TbGdFeCo film is $B_{z,rms}/B(y) \sim 4 \times 10^{-2}$ which compares poorly with the current generation of lithographically fabricated wire atom chips $B_{z,rms}/B(y) \sim 1 \times 10^{-4}$ [18], highlighting the need for further work to improve magnetic materials used in these applications.

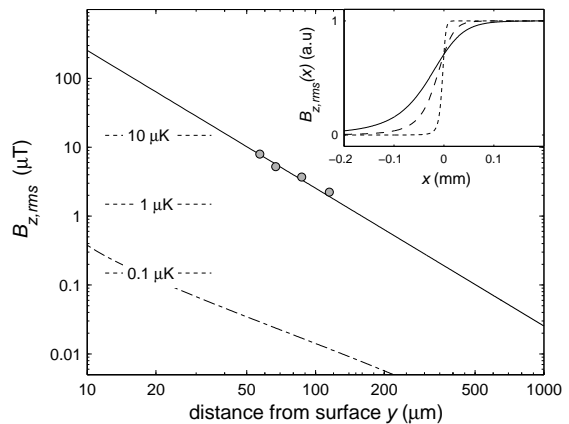


FIG. 4: Behavior of the magnetic field roughness $B_{z,rms}$ as a function of distance from the film surface. The dashed line corresponds to the situation of a homogeneous film with a fluctuating edge as measured by a profilometer. The solid line is a fit to the data using Eq. 4 which corresponds to white noise magnetization variations within the body of the film with a characteristic feature size $d = 5 \mu\text{m}$ and $\Delta M/M_s \simeq 0.3$. The inset shows the predicted x dependence of the field roughness away from the film edge for distances of $y = 10 \mu\text{m}$ (dotted), $y = 50 \mu\text{m}$ (dashed) and $y = 100 \mu\text{m}$ (solid line).

We have found that the amplitude of the corrugated potential is not consistent with magnetostatic calculations based on fluctuations of the film edge (Fig. 4), suggesting that the cause of fragmentation may be spatial variations of the magnetization within the body of the film. To investigate this, a second bias field is applied in the y direction to bring the trap closer to the surface while keeping a constant distance from the edge of the magnetic film. A cloud of atoms positioned $50 \mu\text{m}$ from the surface of the magnetic film and $100 \mu\text{m}$ from the edge is significantly fragmented, while a cloud positioned $50 \mu\text{m}$ from the non-magnetic gold film does not exhibit atomic density variations. This observation confirms that the magnetic field variations originate from the magnetic material itself and not from imperfections along the edge of the film.

Our model describes the effect of two-dimensional spatial variations in the perpendicular magnetization $M_y(x, z)$ of the film. Inhomogeneity leads to the appearance of a random magnetic field above the surface, of which we are most interested in the magnetic field component $B_z(x, y, z)$ that corrugates the bottom of the trapping potential. Using a standard approach incorporating the two-dimensional Fourier transform of the random magnetization $N(k_x, k_z)$ and the magnetic scalar potential we obtain an expression for the B_z component of the corrugated magnetic field. In the case of a magnetic film occupying a half-plane with the edge at $x = 0$ (Fig. 1) and arbitrary magnetization noise we have, for

heights greater than the film thickness,

$$B_z = i2\pi\mu_0y\delta \int_{-\infty}^{\infty} \int_{-\infty}^{\infty} dk_x dk_z k_z^2 N(k_x, k_z) e^{i2\pi(k_x x + k_z z)} \\ \times \int_{-x}^{\infty} dx' e^{i2\pi k_x x'} \frac{K_1(2\pi k_z \sqrt{x'^2 + y^2})}{\sqrt{x'^2 + y^2}}, \quad (3)$$

where δ is the film thickness and K_1 is the modified Bessel function of the second kind. In general this expression can be used to describe any planar pattern of elements that can be represented as a linear combination of step functions.

In the case of white noise fluctuations in the magnetization, $|N(k_x, k_z)| = \text{const}$, the *rms* value of the magnetic field roughness can be evaluated analytically. We perform ensemble averaging and find

$$B_{z,rms} = \sqrt{\frac{3}{\pi} \frac{\mu_0 d \delta \Delta M}{16y^2}} \sqrt{1 + \frac{15}{8}\alpha - \frac{5}{4}\alpha^3 + \frac{3}{8}\alpha^5}, \quad (4)$$

where $\alpha = x/\sqrt{x^2 + y^2}$, ΔM is the *rms* magnetization inhomogeneity and d is the characteristic feature size of the domain structure. For $x = 0$ the model predicts that the corrugated magnetic field component decays with a y^{-2} dependence, consistent with our experimental result. This behavior can also be compared with the more rapid decay ($\propto y^{-2.5}$) expected for white noise fluctuations of the edge of current-carrying wires [16, 17]. Film edge fluctuations are expected to produce corrugations three orders of magnitude smaller than that observed in the experiments (Fig. 4). The model also predicts the fast decay of the corrugated magnetic field away from the film edge for $x < 0$ (Fig. 4-inset).

In Fig. 4 the experimental results are compared with the model with relevant energy scales indicated by dotted lines. The characteristic feature size and distribution function of the domain structure has been inferred from MFM measurements of a demagnetized TbGdFeCo film and is found to have close to white noise characteristics with $d \approx 5 \mu\text{m}$. The best fit of Eq. (4) to the data is found

for $\Delta M/M_s \simeq 0.3$ where M_s is the saturation magnetization of the film. If the inhomogeneity is assumed to originate from reversal of a small number of magnetic domains ($M_y(x, z) = \pm M_s$) then we conclude that the mean magnetization of the film is greater than $0.9M_s$.

The TbGdFeCo magnetic film was originally chosen for its desirable magnetic properties including a large coercivity ($\mu_0 H_c = 0.32$ T) and a high Curie temperature ($T_c \sim 300^\circ\text{C}$) [22]. We attribute the observed inhomogeneity to deterioration of the magnetic film experienced during the vacuum bake-out (140°C over 4 days) despite the relatively high Curie temperature of our film. This conclusion is consistent with reports of reduced perpendicular anisotropy found for similar films after annealing at temperatures above 100°C [33, 34] and with our own measurements on similar films.

In conclusion, trapped ultracold atoms are very sensitive to small magnetic field variations found near the surface of the permanent magnetic film. These variations corrugate the longitudinal trapping potential and result in fragmentation of atomic density. We have developed the technique of spatially resolved rf spectroscopy as a powerful method for accurately mapping small magnetic field variations near the surface of the magnetic film. A simple model accounts for spatial inhomogeneity of the film magnetization and agrees well with the observations. The development of new permanent magnet atom chips will require additional research aimed at further optimizing the quality of magnetic films.

Acknowledgments

We would like to thank J. Wang for the deposition of the magnetic film. T. Roach acknowledges the Donors of the American Chemical Society Petroleum Research Fund for support during this research. This project is supported by the ARC Centre of Excellence for Quantum-Atom Optics and a Swinburne University Strategic Initiative grant.

-
- [1] R. Folman, P. Krüger, J. Schmiedmayer, J. Denschlag, and C. Henkel, *Adv. At. Mol. Opt. Phys.* **48**, 263 (2002).
 - [2] W. Hänsel, P. Hommelhoff, T. W. Hänsch, and J. Reichel, *Nature (London)* **413**, 498 (2001).
 - [3] H. Ott, J. Fortágh, G. Schlotterbeck, A. Grossmann, and C. Zimmermann, *Phys. Rev. Lett.* **87**, 230401 (2001).
 - [4] A. E. Leanhardt, A. P. Chikkatur, D. Kielpinski, Y. Shin, T. L. Gustavson, W. Ketterle, and D. E. Pritchard, *Phys. Rev. Lett.* **89**, 040401 (2002).
 - [5] P. Hommelhoff, W. Hänsel, T. Steinmetz, T. W. Hänsch, and J. Reichel, *New J. Phys.* **7**, 3 (2005).
 - [6] Y. Shin, C. Sanner, G. B. Jo, T. A. Pasquini, M. Saba, W. Ketterle, D. E. Pritchard, M. Vengalattore, and M. Prentiss, *Phys. Rev. A* **72**, 021604(R) (2005).
 - [7] T. Schumm, S. Hofferberth, L. M. Andersson, S. Wildermuth, S. Groth, I. Bar-Joseph, J. Schmiedmayer, and P. Krüger, *Nature (London)* **1**, 57 (2005).
 - [8] A. I. Sidorov, R. J. McLean, F. Scharnberg, D. S. Gough, T. J. Davis, B. A. Sexton, G. I. Opat, and P. Hannaford, *Acta Phys. Pol. B* **33**, 2137 (2002).
 - [9] C. D. J. Sinclair, E. A. Curtis, I. L. Garcia, J. A. Retter, B. V. Hall, S. Eriksson, B. E. Sauer, and E. A. Hinds, *Phys. Rev. A* **72**, 031603(R) (2005).
 - [10] M. Vengalattore, R. S. Conroy, W. Rooijackers, and M. Prentiss, *J. Appl. Phys.* **95**, 4404 (2004).
 - [11] I. Llorente-Garcia, C. D. J. Sinclair, E. A. Curtis, S. Eriksson, B. E. Sauer, and E. A. Hinds, *J. Phys.: Conf. Ser.* **19**, 70 (2005).
 - [12] M. Boyd, E. W. Streed, P. Medley, G. K. Campbell, J. Mun, W. Ketterle, and D. E. Pritchard, cond-

- mat/0608370 (2006).
- [13] B. V. Hall, S. Whitlock, F. Scharnberg, P. Hannaford, and A. Sidorov, *J. Phys. B: At. Mol. Opt. Phys.* **39**, 27 (2006).
- [14] A. Jaakkola, A. Shevchenko, K. Lindfors, M. Hautakorpi, E. Il'yashenko, T. H. Johansen, and M. Kaivola, *Eur. Phys. J. D* **35**, 81 (2005).
- [15] I. Barb, R. Gerritsma, Y. T. Xing, J. B. Goedkoop, and R. J. C. Spreeuw, *Eur. Phys. J. D* **35**, 75 (2005).
- [16] D. W. Wang, M. D. Lukin, and E. Demler, *Phys. Rev. Lett.* **92**, 076802 (2004).
- [17] J. Estève, C. Aussibal, T. Schumm, C. Figl, D. Maily, I. Bouchoule, C. I. Westbrook, and A. Aspect, *Phys. Rev. A* **70**, 043629 (2004).
- [18] P. Krüger, L. M. Andersson, S. Wildermuth, S. Hofferberth, E. Haller, S. Aigner, S. Groth, I. Bar-Joseph, and J. Schmiedmayer, *cond-mat/0504686* (2004).
- [19] L. D. Pietra, S. Aigner, C. vom Hagen, H. J. Lezec, and J. Schmiedmayer, *J. Phys.: Conf. Ser.* **19**, 30 (2005).
- [20] C. D. J. Sinclair, J. A. Retter, E. A. Curtis, B. V. Hall, I. Llorente-Garcia, S. Eriksson, B. E. Sauer, and E. A. Hinds, *Eur. Phys. J. D* **35**, 105 (2005).
- [21] B. V. Hall, S. Whitlock, F. Scharnberg, P. Hannaford, and A. Sidorov, in *Laser Spectroscopy XVII*, edited by E. A. Hinds, A. Ferguson, and E. Riis (World Scientific, Singapore, 2005).
- [22] J. Y. Wang, S. Whitlock, F. Scharnberg, D. Gough, A. I. Sidorov, R. J. McLean, and P. Hannaford, *J. Phys. D: Appl. Phys.* **38**, 4015 (2005).
- [23] S. Wildermuth, S. Hofferberth, I. Lesanovsky, E. Haller, L. M. Andersson, S. Groth, I. Bar-Joseph, P. Krüger, and J. Schmiedmayer, *Nature (London)* **435**, 440 (2005).
- [24] A. Günther, M. Kemmler, S. Kraft, C. J. Vale, C. Zimmermann, and J. Fortágh, *Phys. Rev. A* **71**, 063619 (2005).
- [25] A. G. Martin, K. Helmerson, V. S. Bagnato, G. P. Lafyatis, and D. E. Pritchard, *Phys. Rev. Lett.* **61**, 2431 (1988).
- [26] K. Helmerson, A. G. Martin, and D. E. Pritchard, *J. Opt. Soc. Am. B* **9**, 483 (1992).
- [27] I. Bloch, T. W. Hänsch, and T. Esslinger, *Phys. Rev. Lett.* **82**, 3008 (1999).
- [28] S. Gupta, Z. Hadzibabic, M. W. Zwierlein, C. A. Stan, K. Dieckmann, C. H. Schunck, E. G. M. van Kempen, B. J. Verhaar, and W. Ketterle, *Science* **300**, 1723 (2003).
- [29] C. Chin, M. Bartenstein, A. Altmeyer, S. Riedl, S. Jochim, J. H. Denschlag, and R. Grimm, *Science* **305**, 1128 (2004).
- [30] O. J. Luiten, M. W. Reynolds, and J. T. M. Walraven, *Phys. Rev. A* **53**, 381 (1996).
- [31] J. Fortágh, H. Ott, S. Kraft, A. Günther, and C. Zimmermann, *Phys. Rev. A* **66**, 041604(R) (2002).
- [32] B. V. Hall, S. Whitlock, R. Anderson, P. Hannaford, and A. Sidorov, *cond-mat/0609014* (2006).
- [33] F. E. Luborsky, *J. Appl. Phys.* **57**, 3592 (1985).
- [34] Y. J. Wang and Q. W. Leng, *Phys. Rev. B* **41**, 651 (1990).